PCCP

Accepted Manuscript

ROYAL SOCIETY OF CHEMISTRY

www.rsc.org/pccp

ARTICLE TYPE www.rsc.org/xxxxxx | XXXXXXXX

Chemical interaction of water molecules with framework Al in acid zeolites. A periodic ab initio study on H-Clinoptilolite.

Karell Valdiviés-Cruz,[a] Anabel Lam[a] and Claudio M. Zicovich-Wilson[*b]

Received (in XXX, XXX) Xth XXXXXXXXX 200X, Accepted Xth XXXXXXXXX 200X
First published on the web Xth XXXXXXXXX 200X
DOI: 10.1039/b00000000x

Periodic quantum-chemistry methods as implemented in the CRYSTAL14 code were considered to analyse the interaction of acid Clinoptilolite with water. Initially adsorbed molecules hydrolyse the Al-O bonds, giving rise to defective dealuminated materials. A suitable and representative periodic model of the partially disordered hydrated H-zeolite is the primitive cell (18 T sites) of a decahydrated trialuminated structure of HEU topology. The water distribution inside the material cavities was initially investigated. The model considered for further dealumination was the most stable one from those generated through a combined force field Monte Carlo and ab initio optimization strategy. Optimizations and energy estimations were made at the hybrid DFT level of theory (PBE0 functional) with an atomic basis set of VDZP quality. The energetic of the different pathways involved in the dealumination process was addressed by considering the Gibbs free energy with thermal and zero-point corrections through phonon analysis. It arises that hydrated models exhibit protonated water clusters stabilized by different kinds of H-bonds. The first Al extraction is slightly more energetically favourable from T_3 than T_2 sites, but at the same time the latter is more probable owing to its larger Al population. However, concerning the second dealumination step, it is more favourable removing the Al atom from both remaining sites after a starting abstraction from T_2 rather than T_3. These facts determine that the most probable overall pathways go through a first Al removal from T_2. The agreement with experimental results is discussed.

1. Introduction

Zeolites are solids with microporous structure technologically employed as catalysts, effective adsorbents and molecular sieves.[1] The use of natural zeolites to such scopes is economically competitive as they are easy to extract and they are also present on earth in huge quantities. Nonetheless, the main problem is the small pore diameter of these materials that makes difficult the efficient adsorption of medium/large molecules inside channels and cavities. As a way to exploit the former advantages avoiding the latter problems, structural modification techniques through chemical modification of natural zeolites [2,3] have been proposed so as to develop new materials not much expensive and suitable for industrial use. An effective procedure currently employed for such a purpose is dealumination. This consists of successive abstraction of aluminum atoms from the framework by means of acid treatments,[4,5] leaving silanol nests that enlarge cavities. The procedure allows obtaining molecular sieves with pores large enough so as to admit efficient diffusion of relatively large molecules.

Clinoptilolite is the most abundant zeolite on nature. Its crystalline structure was refined by Alberti *et al.* [6] in a monoclinic cell with C 2/m space group. The framework is of HEU type. The conventional cell parameters are: a=17.64 Å, b=17.89 Å, c=7.39 Å, β=116.22°, [4] which corresponds to a primitive cell with a=12.41 Å, b=12.57 Å, c=7.28 Å, α=69.04°, β=105.58° and γ=88.38°. There are three channels in clinoptilolite disposed in two dimensions. Channels *a* and *b* run along the c axis and exhibit 8- and 10- member rings, respectively. On the other hand, channel *c* also displays 8-MR and goes parallel to the a axis. About twenty water molecules per unit cell may be occluded into such channels. Several types of compensation cations like Na^+, K^+ and Ca^{2+} may also appear.[7]

In Fig. 1 the acid clinoptilolite is shown, according to the structure reported in Ref. [8]. For the sake of simplicity water molecules, as well as acidic protons have been omitted.

Aluminum atoms occupy the five topologically distinct tetrahedral sites of the framework, namely T_i (i=1-5).[6] Each site exhibits a different aluminum occupation that depends on the nature of the compensation cations in the material. For instance, in samples where sodium is the prevailing compensation cation, the average occupation of Al atoms per site is the largest one at T_2 followed by T_3, taking values of about 40 and 20 %, respectively. [6,9] In a so much lower amount, they occupy T_5 and T_1 and are practically absent at T_4. As concerns the Si/Al ratio it exhibits a value slightly above 4.0.

Dealumination of acid Clinoptilolite in acid media occurs in approximately 1 h at room temperature. Clinoptilolite can be dealuminated up to 46% of the original Al content without perceptible crystallinity loss, yielding a thermally stable material. [10] An analysis of the ^{27}Al NMR spectra allows to detect an increase in the amount of octahedral Al upon dealumination together with a simultaneous decrease of such a cation in tetrahedral coordination.[8,10] This is to be taken as a symptom of the removal of Al from framework and subsequent formation of extraframework species inside the cavities.[10] It has been proven that, at variance with the starting acid Clinoptilolite, such a modified material can be employed for technological purposes as for instance the separation of n-paraffins by diffusion.[11]

The use of experimental techniques to understand the mechanisms involved in the hydrolysis of Al-O bonds that occurs during dealumination is a very complex and costly task. On the contrary, the consideration of computational techniques to this scope appears to be an appealing alternative. In the last years some theoretical works have been performed to study the processes involved in the dealumination of different zeolitic

frameworks.[12,13] Nevertheless, the influence of Al location and local environment in the efficiency of the several steps of the reaction still deserves elucidation.

In a previous work of some of us [8] the energetics involved in the complete dealumination of acid clinoptilolite at DFT level (PBE functional) was considered. Such a study suggested that Al atoms located at T_2 sites are more favourable for removal than those at T_3. In that work, a conventional cell of HEU topology was considered for computational simulations and not all dealumination pathways were explored. In addition, the values of energy involved in the different pathways were not computed including thermal effects, so that those results are not fully comparable with experimental data.

A more recent work [14] has been devoted to investigate the best models and methodologies to be employed for the study of zeolites with HEU topology with different Al loading and water content. It was shown that PBE0 functional within the hybrid-DFT approach reasonably reproduces most structural and energetic features of such a family of compounds. The influence of hydration on the local structure of HEU type models has been also considered and it turns out that different kinds of H-bond interactions connect occluded water molecules to each other and the zeolitic inner walls. These interactions appear to stabilize the framework Al sites.[9] The stabilization is larger for Al at T_2 than at T_3 which is consistent with the fact that the former is practically twice as populated by Al atoms than the latter in the natural material. Such a study, however, was mainly focused on methodological issues and general effects of hydration in H-Clinoptilolite. Accordingly, unrealistic low water content models were there considered.

In the present work, we are interested in: (a) generating a realistic and, at the same time, computationally affordable model for hydrated H-Clinoptilolite and studying the influence of hydration on its structural features, and (b) investigating the energetics of all possible dealumination pathways from such a model. To these purpose we have employed periodic quantum chemical methods at hybrid-DFT level as implemented in the CRYSTAL14 code. [15,16]

2. Computational details

Electronic structure calculations have been performed by considering the PBE0 approach.[17] As stated in a previous work, [18] inclusion of long-range van der Waals forces is in general mandatory to reasonably reproduce cell parameters and stability trends in DFT calculations of Si-zeolites with different density. Such a correction is actually possible in LCAO periodic calculations, [19,20] but it requires a substantially high basis set level, a fact that would make extremely expensive the computational cost of the present work. However, in our previous methodological study on H-Clinoptilolite [14] it was shown that, being PBE0 one of the DFT approaches that less amount of dispersion correction requires, it provides reasonable structural results at a basis set level not as costly as to allow a quite rich study with accessible computational resources.

The considered basis set is a valence double-ζ with polarization (VDZP) one. The Hamiltonian matrix have been diagonalized in a set of k-points in reciprocal space generated according to the Pack-Monkhorst prescription [21] for sampling the first Brillouin Zone (BZ) with shrinking factor 2. This gives rise to 8 k-points as all models considered exhibit P1 space symmetry. The tolerances considered for the computation of mono and bi-electronic integrals employed in the coulomb and exchange series were those recommended in the code manual.[15] The exchange-correlation contribution has been numerically integrated considering a pruned grid with 75 points in the radial and a maximum of 434 points in the angular parts around the nuclei (see keyword LGRID in the code manual).[15] The condition for convergence of the SCF part was that the energy difference between two subsequent cycles must be less than $1x10^{-7}$ Hartree. The same overall computational conditions have been validated in a previous work for the study of hydrated models for H-Clinoptilolite.[14]

Geometry optimizations were performed with analytic gradients for both atomic positions and lattice parameters, and a pseudo-Newton algorithm (BFGS) for Hessian matrix update.[15] Convergence was tested by considering the default thresholds recommended in the code manual.[15] In order to ensure consistency between the final geometry and the approximations considered for integral evaluation, the FINALRUN option of the code with value 4 has also been employed.[15]

The Gibbs free energy (G) of all minima at 298 K and 1 atm has been computed by just considering vibration thermal contributions through phonon calculations at Γ-point of the BZ. Given the large size of the unit cell it is expected the considered sampling to be enough for a reasonable description of the thermodynamic state function differences here taken into account.

The models of hydrated H-Clinoptilolite considered for calculations have two Al atoms in T_2 and one in T_3 positions considering the HEU primitive cell. This reasonably mimics the framework cation distribution of experimental H-Clinoptilolite, as discussed elsewhere.[14] Acidic protons are positioned on O-bridging atoms at positions 4 and 2 (according to the notation proposed in Ref. [6]) around framework Al in T_2 and T_3, respectively.[14]

Ten water molecules, about three per each acid site, were accommodated in the cavities of the anhydrous material, by means of a Monte Carlo sampling in a NVT ensemble at 300 K with periodic boundary conditions and Universal Force Field.[22] It is well known that such a classical force-field is not well enough suited to study systems with many H-bonds.[22] It is then expected that the obtained energy values to be in general rather different than those coming from electronic structure calculations at the level here considered. Nevertheless, the present approach is extremely useful in practical terms as the Monte Carlo sampling at classical force-field level allows efficiently exploring a huge number of reasonably represented configurations. This permits a quite good thermostatistical description of the system. After the selection performed, the lack in the accurate description of the energetics associated to the use of a force-field approach is corrected in a large amount by geometry optimizations of the chosen structures performed at the DFT level previously mentioned.

From the 10^6 generated configurations the three most stable ones (under the force-field estimation) have been chosen. These geometries were classified according to the water distribution

inside 8- and 10-MR channels (*a* and *b,* mentioned in the Introduction) in the resulting structures. The classes considered are: five water molecules in each channel (type 1), four and six in the former and the latter, respectively (type 2), and the converse situation (type 3). The selected models were subsequently optimized at the hybrid DFT level above mentioned. The resulting models are here labelled as HT[10]-N, where index N=1,2,3 corresponds to the previously mentioned classification and 10 refers to the water content. The structures consist of 87 atoms per primitive cell.

It arises that the considered H-CLI models displays a large number of degrees of freedom, so that their Potential Energy Hyper-surfaces should exhibit several minima. The complexity of the system calls for the use of statistical simulations such as Born-Oppenheimer Molecular Dynamics at the present computational level. However, in order to get results accurate enough to reach statistical validity, large simulation times must be considered making the whole set of required calculations extremely expensive. The alternative strategy here adopted and previously tested,[14] allows a reasonable exploration of the different possible configurations and a thermostatistical estimation of the Gibbs free energy of the most probable structures through the above discussed combination of classical force-field Monte Carlo techniques and energy optimisations plus phonon hybrid-DFT calculations, respectively.

Gradual Aluminum removal from framework was achieved by throwing off one Al atom in each step. The dangling bonds of the three starting O-bridging atoms were saturated with hydrogen ones that, together with the original acidic OH form a silanol nest [≡$(SiOH)_4$]. Those groups result from the simultaneous dissociation of three water molecules together with the formation of $Al(OH)_3$. In a similar way, the first, second and third Al removal steps give rise to dialuminated, monoaluminated and pure silica models, respectively. Such models exhibit seven, four and one water molecules, and consist of 80, 73 and 66 atoms per unit cell, respectively.

It is worthwhile noting that those water molecules more involved in the formation of the silanol nest at a given T site are the nearest ones to the Al atom being removed. Accordingly, one can assume that they dissociate and hydrolyse the Al-O bonds, disappearing in each step from the reaction mixture. Such a procedure does not warrant the resulting Si-OH are oriented in the most stable direction in the formed nests. Despite this, it provides reasonable representations of sets of energetically differing configurations. As shown in what follows, their characterization allows obtaining very useful information on the actually disordered systems.

In the actual dealumination reaction, a polymeric compound of composition $Al_2O_3(H_2O)_n$, where n is a variable quantity, is formed in the cavities as a product. This contains the so-called extra-framework Al cations. It is known that such cations, at variance with framework ones, mostly exhibit octahedral coordination. Nonetheless, being a disordered system its structural details are still unknown. This is the reason why it is very difficult to design suitable structures to model the product of the dealumination reaction so as to carry out electronic structure calculations to evaluate the reaction energy corresponding to each step. Accordingly, in this work reaction energies were not explicitly computed. The relative stability of the different possible intermediates in the same dealumination step is considered in the analysis instead.

In Fig. 2, a scheme of the possible pathways involved in the complete dealumination of the considered HEU model is shown. As it turns out from figure, in the first removal step three different intermediates are involved. Meanwhile, in the second and third steps six products result. Such intermediates were labeled as follows: HD[7](s_1), HM[4](s_1s_2) and PS[1]($s_1s_2s_3$), respectively. The labels s_1, s_2 and s_3 refer to the first, second and third framework sites, respectively, where dealumination occurs. As in the hydrated models the number within square brackets indicates the water content per unit cell. The T_2 sites are identified according to their position relative to T_3: the closest and the furthest ones are labelled as "neighbouring" (2_n) and "remote" (2_r), respectively.

The six final geometries correspond to different conformations of the same pure silica material. This is substantially due to the way silanol groups and water atoms arrange in dependence of the sequence of reaction pathways that lead to the final product. Indeed, such a system was not experimentally characterized as actually the framework collapses before the full dealumination is reached. The collapse does not occur in computational simulations because models are forced to keep a periodic arrangement. Therefore they are unable to feature the amorphization that must accompany the process. The electronic-nuclear and Gibbs energy values for the different geometries arising from each removal step have been also calculated.

Basis set superposition error (BSSE) corrections were performed at this level for water adsorption energy, by adopting the Counterpoise scheme.[23] The magnitude of the correction for a single water molecule was here estimated by considering the desorption of the whole water content divided by the number of molecules. The chosen set correspond to the most stable model. It is assumed that, in spite of the somehow arbitrary procedure, it provides in general a reasonable estimation of the adsorption energy.[14]

3. Results and discussion

3.1 Decahydrated acid trialuminated HEU models

The optimized geometries of the three considered models for hydrated H-Clinoptilolite are shown in Figure 3. As it turns out from figure, in models HT[10]-2 and HT[10]-3 some water molecules migrate from the original location in the 8-MR channel toward the 10-MR one in the final arrangement. Accordingly, the three models reach similar water distributions. In addition, it arises that molecules in general prefer to be disposed around T_2 sites. As previously suggested, [14] this is likely due to the difference in framework constrains in each case. It turns out that such a site shares a lower number of framework 4-MR than T_3, so it experiments less local strain promoted by the environment. This allows the environment of Al atoms located at T_2 to be much more free for rearrangement and coordination with water molecules than those around Al at T_3.

In all considered models, a transfer of a couple of protons from the acid sites to the water molecules residing inside the channels occurs. In our previous study,[14] where the

considered models exhibited a significantly lower water content than in the present work (three molecules per primitive cell), such a proton transfer from the acid sites to the occluded water molecules and the resulting formation of charged clusters did not take place. According to previous works [13,24-28] the present study provides strong evidences that the deprotonation of the Brönsted site depends on the number of water molecules inside the cavities. This is likely due to the local changes in the framework induced by the interaction through H-bonds of the molecules and the channel surfaces. The proton transfer process brings about the formation of occluded cationic water clusters in which several molecules share the proton providing an important stabilising role. For instance, in HT[10]-1 two $H_5O_2^+$ clusters are formed, while in HT[10]-2 and HT[10]-3 two $H_7O_3^+$ ones appear.

The optimized lattice parameters of the three hydrated models together with the corresponding average bond distances and angles are documented in Tables SI-1, SI-2 and SI-3 (see SI). In general, it turns out that calculated lattice parameters and bond distances are acceptable in comparison with the experimental ones.[29,30] Interestingly, the obtained average T_3-O bond distances (T=Al) are slightly lower than the corresponding T_2-O ones. This effect may be connected to the above mentioned difference in framework constrains between both sites that allows much more structural relaxation in the latter than in the former.

Table 1 reckons the total energy of the three hydrated models relative to the most stable one, ΔE, the Gibbs free energy, ΔG, and the hydration energy and Gibbs hydration free energy values without and with BSSE correction, respectively. The latter correction term was just estimated for the most stable model, namely HT[10]-1, resulting in 5.6 kcal/mol per water molecule.

The hydration energy, ΔE_H, was computed according to:

$$\Delta E_H = [E_{Z\text{-}w} - (E_Z + nE_w)]/n \qquad (1)$$

where $E_{Z\text{-}w}$, E_Z and E_w are the energies of the hydrated and the anhydrous zeolitic models, and the isolated water molecule, respectively; n is the number of occluded water molecules, in the present case n = 10. Equation (1) quantifies the reaction energy (per water molecule) according to the following scheme:

$$HT + 10\ H_2O \longrightarrow HT[10]\text{-}N \qquad (2)$$

here HT is the starting anhydrous H-CLI model. The Gibbs hydration free energy is computed in the same way as in (1).

The different values of Gibbs hydration energy per water molecule (ΔG_H) are very close to each other, but they follow the same trend as ΔG. Let us now try interpreting such a trend in terms of the way water molecules and charged interact with the framework and to each other. A similar strategy has been considered in a previous work with successful results.[14]

In all models, the formation of different kinds of H-bonding is observed. Some overall structural results connected to the H-bonds featured between water molecules and charged clusters occluded inside the channels of the models are listed in Table SI-4. The H-bonds are classified according to the expected decreasing strength and in a similar way as in our previous work. [14] See Table SI-4 in the SI file for more information. Nevertheless, in the present work a new type of H-bond, referred to as class (II) is included. This group includes those water molecules H-bonded to each other to form cationic water clusters. The criterion considered for identifying an H-bond is that the OH distance should be shorter than 2.1 Å. Likewise, in Tables SI-5 and SI-6 the detailed O…H, as well as the Mulliken charges of the H and O atoms involved in the interactions are also documented (see SI). All these interactions do contribute to the stabilization of the hydrated models under study.

As it arises from Table SI-4, all models exhibit similar values for the average H-bond distance (see SI). On the other hand, no clear correlation between number and type of H-bonds and the stability of the models can be straightforwardly drawn. This is consistent with the fact that all of them display similar hydration energy and can be roughly considered as equivalent from the chemical point of view. It arises that the accomodation of ten water molecules per u. c. inside the zeolite exhibits a noticeable increase in the number of H-bonds as compared with previous results considering just three ones. In that work,[14] it was possible to explain the stability order of the hydrated H-CLI models in terms of a classification of H-bond interactions. Nonetheless, in the present case the appearance of new phenomena makes the H-bond interactions to be intermingled in a complex manner, so that it is not easy to correlate them in a convincing way.

In Table SI-7 a brief information of the framework constraints imposed on the O atoms that form H-bonds with the occluded molecules and cationic clusters is provided (see SI). In accordance with the classification shown in Table SI-4, when water molecules and cationic clusters adsorb on O atoms belonging to deprotonated Brönsted sites, H-bonds of type (III) give rise to an average decrease of the Al-O distance of 0.07-0.13 Å with respect to the corresponding anhydrous zeolite, as it turns out from Table SI-7. This suggests an enhancement of the bond rigidity of the AlO_4 tetrahedra and so the site becomes much more strained (and less stable) upon deprotonation and subsequent water adsorption. In adsorptions involving the remaining cases of O atoms in Al-O-Si bridges, the presence of H-bonds of type (III) brings about an enlargement of the Al-O bonds of about 0.01-0.06 Å. At variance with the previous case, this reflects the increase of the ionic character of the bond, making the AlO_4 tetrahedron slightly more flexible and allowing some additional relaxation when the adsorption site is part of 4-MR building units.[31] Though water adsorption on Al-O-Si bridges provides a general stabilising effect, one thus expects that this should be less pronounced when occurring on a deprotonated Brönsted site that at the same time belongs to a 4-MR than in other cases.

Taking into account these considerations let us now try to interpret the stability trend exhibited by the considered models. As it turns out from Table SI-7, the two most stable systems, HT[10]-1 and HT[10]-3, display four 4-MRs involved in H-bonds of type (III). Nevertheless, in the former just one of them includes a deprotonated acid site, while in the latter there are two of them. Accordingly, HT[10]-1 should become much more stabilized upon the adsorption of water molecules Al-O-Si bridges than HT[10]-3. Finally, as concerns the least stable model, HT[10]-2, it displays only two 4-MR involved in Al-O-Si bridges that exhibit H-bonds of type (III) and one of them belongs to a

deprotonated acid site. Such details could explain its slightly lower stability respect to the others.

As it turns out from the previous discussion, the high complexity of the actual models makes not as straightforward as in Ref. [14] to correlate the slight differences in stability of the hydrated H-CLI models in terms of H-bond interactions, framework topology and other structural features. This is due to the increase of the statistical character of the processes that occur in the studied zeolitic materials as the number of water molecules increases too.

3.2 Dealumination in H-Clinoptilolite

The optimized structures obtained for the different dealumination pathways (see Fig. 2) considering as starting species the most stable model of hydrated H-Clinoptilolite, HT[10]-1, are shown in Fig. 4. As it was stated in Sec. 2, when an Al atom is removed from the framework, three water molecules must dissociate to bring about a silanol nest together with an $Al(OH)_3$. At the same time, the remaining water molecules and cationic clusters are redistributed in the cavities. Upon the third reaction step, purely silicic compounds are formed. Since such structures are different configurations of the same material, for the sake of simplicity, only the geometry of the most stable one is here documented.

Let us first consider the changes featured by water molecules occluded inside the zeolitic channels during the different pathways shown in Fig. 4. In the first reaction step, when Al atoms at either T_3 or T_{2r} sites are abstracted, the acidic proton in the neighbour of T_{2n} is always transferred to a water cluster. This might be a consequence of the slight acidity enhancement connected to the Si/Al ratio increase upon dealumination. Moreover, the two $H_5O_2^+$ clusters originally residing in the channels of HT[10]-1 are still present in such intermediates.

In the second reaction step, only a single $H_5O_2^+$ cluster remains in HM[4](2_r2_n), HM[4](2_n2_r) and HM[4](2_n3) (see Figs. 4d, 4f and 4g, respectively). On the other hand, in HM[4](2_r3) just one $H_7O_3^+$ cluster can be found (see Fig. 4e). In HM[4](32_n) and HM[4](32_r) a proton transfer from the cationic water clusters to one T_2 site is observed, so as the Brönsted site is regenerated (see Figs. 4h and 4i). This contributes to a reduction of the charge separation among the $H_7O_3^+$ clusters and the deprotonated O-bridging adjacent to T_2 sites in HD[7](3). In addition, it suggests a loss of acidity in the T_2 site, opposite to the increase observed upon the first dealumination step, is taking place. It is likely that this is the result of the concurrence of two global effects that go contrariwise in what concerns their influence on the zeolite acidity. They are the above mentioned Si/Al ratio and the number of silanol groups, both ones increasing upon dealumination. Concerning the latter, one can assume that the formation of silanol nests provides an inductive effect similar to that exhibited by framework Al atoms that tend to decrease the overall acidity of the material. It appears that the effect of the presence of silanol groups becomes dominant in the last stages of dealumination giving rise to an overall loss of acidity. This is reflected in the featured recovering of the proton by the Brönsted site upon the second step.

In Table 2 the electronic-nuclear energy, ΔE, as well as the Gibbs energy, ΔG, for each intermediate of the dealumination reaction of HT[10]-1 are documented. The reported values are relative to the most stable model in each step. The results for the third dealumination step have been excluded as it does not experimentally take place.

It arises from ΔG values in Table 2 that in the first reaction step the Al atom removal from either T_{2r} or T_3 sites requires rather similar energy cost, with a very small difference favouring the latter. However, it is worthwhile noting that the relationship between Al occupancies in T_2 and T_3 is practically two in both experiments and models. Therefore, removing one Al atom from T_2 is the most probable event despite the slight energy difference in favour of the Al abstraction from T_3. In a previous work [8] it was shown that abstraction of the first Al atom from a T_2 site in H-Clinoptilolite is the most favourable event in agreement with the present results. On the other hand, it arises from the energetic results given in Table 4 that removal of one Al atom from both remaining sites in the second step is more favourable when the first Al abstraction was from T_2 than T_3 sites. It is then expected that the most probable overall pathways for the first and second dealumination steps go through a first Al removal from T_2, particularly T_{2r}.

The stability order exhibited by the structures involved in each reaction step according to their Gibbs free energy values is as follows:

Step 1: HD[7](3)~ HD[7](2_r)> HD[7](2_n)

Step 2: HM[4](2_n2_r) ~ HM[4](2_r3)~ HM[4](2_r2_n)> HM[4](2_n3)> HM[4](32_n)> HM[4](32_r)

Table SI-8 reckons the lattice parameters of the original model, HT[10]-1, as well as the corresponding ones for the different intermediates in the dealumination reaction (see SI). For the third step, the values referred to the most stable purely silicic model, namely PS[1](2_r2_n3), are the only ones reported just for the sake of comparison but according to the above stated criterion that concerns the lack of correspondence with experimental data. Additionally, Tables SI-9 and SI-10 document the average bond distances and angles corresponding to the different intermediates of the dealumination of HT[10]-1 (see SI).

As it turns out from Table SI-8, when an Al atom is removed from framework T_{2r} or T_3 sites, lattice parameter b decreases, leading to a cell volume contraction. This fact was previously reported in experimental works. [10,11] Nevertheless, when the Al atom is taken away from T_{2n}, the converse situation occurs. It is worthwhile noting that the product of the latter reaction, HD[7](2_n), is the least stable one among the different possibilities considered for the step. This suggests that the above mentioned volume contraction is somehow connected to structural features that bring about a stability loss of the overall system. This is discussed in what follows.

In Table SI-11 a selection of data is provided that concerns some relevant features of the H-bonds in the models considered for the different stages of the dealumination process (see SI). The classification of the interactions follows similar criteria as considered in Table SI-4. In this case the presence of silanol groups in the dealuminated models requires the inclusion of a new type of H-bond. This, referred to as class (V), includes those H-bond interactions among silanol groups and both water

molecules and protonated water clusters occluded within channels. These are expected to be the weakest interactions among those here considered. Additionally, Table SI-12 and SI-13 document detailed O…H distances, as well as Mulliken charges on the H and O atoms involved (see SI).

Particular topological information concerning the 4-MRs involving framework O atoms in Al-O-Si bridges and being simultaneously coordinated to water molecules and cationic clusters, is shown in Table SI-14. Note that HM[4](2$_r$3), HM[4](2$_n$2$_r$) and HM[4](32$_n$) are not documented in Table as such models display no situations of this kind. It arises from Table that when water molecules interact with O atoms from clean Al-O-Si bridges in the original anhydrous material, this situation gives rise to an enlargement of the Al-O bonds in the range of 0.01-0.09 Å. Such an enlargement is accompanied by an increase of the ionic character of the T-O bonds (see Table SI-14 in SI file), a fact that does allow additional relaxation of the rather strained 4-MR units. Nevertheless, when water molecules are adsorbed on O atoms belonging to deprotonated Brönsted sites, the Al-O bonds shorten in about 0.08-0.12 Å with respect to the anhydrous zeolitic framework. In such cases, the bond turns out to be more rigid, losing most of the flexibility displayed by the AlO_4 tetrahedron when the OH-bridging takes place.

As it was previously discussed in the case of the hydrated H-CLI models, the complexity of the geometries of the dealuminated intermediates makes also difficult to correlate their stability order in terms of the previous H-bonds and topological classification. However the present analysis provides at least a way to understand some general phenomena that occur in this and other related processes in zeolites that involve the breaking of the framework integrity.

Conclusions

In the present work H-Clinoptilolite is considered so as to investigate the interaction of an acid zeolite with water in both situations: chemisorption and hydrolysis of the Al-O bonds to bring about dealuminated materials. As concerns the study of the hydrated zeolite, models with three framework Al atoms, two at T_2 and one at T_3, together with 10 water molecules per primitive cell have been considered. Such models are assumed to have a chemical composition rather similar to the actual material considered in experiments and allow to elucidate particular details concerning the interaction between adsorbed molecules and framework.

It arises that different phenomena take place during water adsorption on the H-Clinoptilolite inner surfaces. They are the physisorption of water molecules on the channel walls, formation of water clusters and proton transfer from acid sites to water molecules and clusters inside the material cavities. The proton transfer has been well described in previous works [24-28] and has been in general attributed to the particular stability of the cationic water clusters when they remain occluded inside the cavities. In the latter, H-bonding of such clusters with the O atoms at the inner surfaces of the material, enhances even more the stability of the overall system. Similar phenomena occur in the partially dealuminated materials.

It is also shown that water molecules inside the zeolitic channels form an entangled network of H-bonding that involves them, the acidic protons and the O atoms at the cavity walls. The interactions are of different magnitude and have been here classified in five types. The energetic differences among different water distributions in the material have been explained on the basis of such a classification and the topological features of the framework around the adsorption sites.

Concerning the different reactions involved in the dealumination of H-Clinoptilolite brought about through the interaction with such occluded water molecules and clusters, it turns out that the ability of the Al atoms to be removed from framework sites strongly depends not only on the topological circumstances of the T-site but also on the composition around it. This is mainly conditioned by the structural constraints imposed by the environment.

According to the energetic point of view, in the first Al removal step it is slightly more favourable abstracting one atom from T_3 than T_2 site. However, in view of the fact that in H-Clinoptilolite the relationship between Al populations on T_2 and T_3 sites is close to 2:1, the converse situation experimentally holds simply from probability reasons. These results are in agreement with those shown in a previous work.[8] Additionally, the abstraction of Al from both remaining sites in the second removal step is energetically more favourable when the vacancy is at T_2 than T_3. Finally, as it arises from the energetic results for both dealumination steps, the most probable overall pathways go through a first Al removal from T_2, particularly T_{2r}.

As concerns the acidic properties of the material, it turns out that in the first dealumination step its Brönsted acidity increases as reflected by the transfer of the proton from the zeolite to the water clusters occluded in the cavities. This seems to be driven by the increase of the Si/Al ratio of the zeolite upon the process. Surprisingly, in the following dealumination step some protons stabilized by occluded water clusters transfer back to some framework Al-O-Si bridges recovering the Brönsted site. This seems to indicate that not only the Si/Al ratio controls the acidity of the dealuminated zeolite but it is the result of a balance between different effects in which the appearance of silanol nests does play a significant role.

Acknowledgements

The authors acknowledge CONACyT for financial support through Project CB-178853. K.V. also acknowledges CONACyT for a doctoral grant.

Author addresses

[a]*Laboratorio de Ingeniería de Zeolitas, Instituto de Ciencia y Tecnología de Materiales (IMRE), Universidad de La Habana, La Habana, 10400, Cuba.*

[b]*Centro de Investigaciones en Ciencias, Universidad Autónoma del Estado de Morelos (UAEM), Av. Universidad 1001, Col. Chamilpa, 62209, Cuernavaca (MOR), México. E-mail: claudio@uaem.mx*

†Electronic Supplementary Information (ESI) available: Optimized lattice parameters, primitive cell volume, bond distances and angles, together with average hydrogen bond distances and Mulliken populations on O and H atoms for HT[10], HD[7](s_1), HM[4](s_1s_2) and PS[1]($s_1s_2s_3$) models. Figures and geometrical information on the framework O atoms coordinated with water molecules in HD[7](s_1), HM[4](s_1s_2) and PS[1]

($s_1s_2s_3$) models are also shown. See DOI: 10.1039/b000000x/

References

1. D. W. Breck, in *Zeolite Molecular Sieves,* Wiley and Sons, New York, 1973.
2. J. C. Groen, L. A. A. Peffer, J. A. Moulijn, J. Pérez-Ramírez, *Microporous and Mesoporous Materials*, 2004, **69**, 29.
3. J. C. Groen, L. A. A. Peffer, J. A. Moulijn, J. Pérez-Ramírez, *Colloids and Surface A*., 2004, **241**, 53.
4. R. M. Barrer, M. B. Makki, *Canad. J. Chem.*, 1964, **42**, 1481.
5. C. V. McDaniel, P. K. Maher, in *Molecular Sieves*; Barrer, R. M. Ed.; Soc. Chem. Ind.: London, 1968; pp 186.
6. A. Alberti, *Tschermaks Mineral Petrogr. Mitt.*, 1975, **22**, 25.
7. C. Baerlocher, W. M. Meier, D. H. Olson, *Atlas of zeolite framework types*; Elsevier: Amsterdam, 2001.
8. A. Rivera, T. Farías, L. C. de Ménorval, M. Autié-Pérez, A. Lam, *J. Phys. Chem. C*, 2013, **117**, 4079.
9. T. Armbruster, M. E. Gunter, *Am. Miner.* 1991, **76**, 1872.
10. Y. Garcia-Basabe, I. Rodriguez-Iznaga, L. C. de Menorval, P. Llewellyn, G.Maurin, D. W. Lewis, R. Binions, M. Autié-Perez, A. R. Ruiz-Salvador, *Microporous and Mesoporous Materials*, 2010, **135**, 187.
11. A. Rivera, T. Farias, L. C. de Ménorval, G. Autié-Castro, H. Yee-Madeira, J. L. Contreras, M. Autié-Perez, *J. Colloid Interface Sci.*, 2011, **360**, 220.
12. S. Malola, S. Svelle, F. Lønstad Bleken, O. Swang; *Angew. Chem.* Int. Ed., 2012, **51**, 652.
13. M. Silaghi, C. Chizallet, E. Petracovschi, T. Kerber, J. Sauer, P. Raybaud, *ACS Catalysis*, 2015, **5**, 11.
14. K. Valdiviés Cruz, C. M. Zicovich-Wilson, A. Lam, *J. Phys. Chem. A*, 2014, **118**, 5779.
15. R. Dovesi, V. R. Saunders, C. Roetti, R. Orlando, C. M. Zicovich-Wilson, F. Pascale, B. Civalleri, K. Doll, N. M. Harrison, I. J. Bush, P. D'Arco.; M. Llunell, M. Causa, Y. Noel, *CRYSTAL14 User's Manual*; University of Torino: Torino, 2014. See http://www.crystal.unito.it.
16. R. Dovesi, R. Orlando, A. Erba, C. M. Zicovich-Wilson, B. Civalleri, S. Casassa, L. Maschio, M. Ferrabone, M. De La Pierre, P. D'Arco, Y. Noël, M. Causà, M. Rérat, B. Kirtman, Int., *J. Quantum Chem.* 2014, **114**, 1287.
17. C. Adamo, V. Barone, *J. Chem. Phys.*, 1999, **110**, 6158.
18. E. I. Román-Román, C. M. Zicovich-Wilson, *Chem. Phys. Lett.* 2015, **619**, 109-114.
19. S. Grimme, *J. Comput. Chem.*, 2006, **27**, 1787.
20. B. Civalleri, C. M. Zicovich-Wilson, L. Valenzano, P. Ugliengo, *Cryst. Eng. Comm.*, 2008, **10**, 405.
21. H. J. Monkhorst, J. D. Pack, *Phys. Rev. B*, 1976, **13**, 5188.
22. A. K. Rappé, C. J. Casewit, K. S. Colwell, W. A. Goddard, W. M. Skiff, *J. Am. Chem. Soc.*, 1992, **114**, 10024.
23. S. Boys, F. Bernardi, *Mol. Phys.*, 1970, **19**, 553.
24. X. Solans-Monfort, M. Sodupe, V. Branchadell, J. Sauer, R. Orlando, P. Ugliengo, *J. Phys. Chem. B*, 2005, **109**, 3539.
25. V. M. Vener, X. Rozansky, J. Sauer, *Phys. Chem. Chem. Phys.*, 2009, **11**, 1702.
26. M. Krossne, J. Sauer, *J. Phys. Chem.*, 1996, **100**, 6199.
27. M. Sierka, J. Sauer, *J. Chem. Phys.*, 2000, **112**, 6983.
28. C. Tuma, J. Sauer, *Chem. Phys. Let.*, 2004, **387**, 388.
29. R. J. Hill, G. V. Gibbs, *Acta Crystallogr. B*, 1979, **B35**, 25.
30. S. B. Hong, S. H. Lee, C. H. Shin, A. J. Woo, L. J. Alvarez, C. M. Zicovich-Wilson, M. Camblor, *J. Am. Chem. Soc.*, 2004, **126**, 13742.
31. A. Damin, R. Dovesi, A. Zecchina, P. Ugliengo, *Surf. Sci.*, 2001, **479**, 253.

Tables

Table 1: Energy, ΔE, and Gibbs energy, ΔG, of the decahydrated acid trialuminated HEU models relative to the most stable one. Hydration energy per water molecule (ΔE_H), Gibbs hydration energy per water molecule (ΔG_H), hydration energy corrected by the BSSE correction, ΔE_H (corr.) and Gibbs hydration energy corrected by the BSSE correction, ΔG_H (corr.). The energy values are in kcal·mol^{-1}.

Model	ΔE	ΔG	ΔE_H H	ΔG_H	ΔE_H (corr.)	ΔG_H (corr.)
HT[10]-1	0	0	-24.1	-11.2	-18.5	-5.6
HT[10]-2	12.9	20.1	-22.8	-9.2	-17.3	-3.6
HT[10]-3	4.7	10.8	-23.7	-10.0	-18.1	-4.5

Table 2: Electronic-nuclear, ΔE, and Gibbs, ΔG, energies for each intermediate involved in the dealumination reaction of HT[10]-1 relative to the most stable model of the corresponding step (see definition in the text). Energies are given in kcal·mol^{-1}.

Step	Model	ΔE	ΔG
1	HD[7](2_r)	9.8	1.2
	HD[7](2_n)	3.5	3.9
	HD[7](3)	0	0
2	HM[4](2_r2_n)	6.8	1.6
	HM[4](2_r3)	6.3	1.1
	HM[4](2_n2_r)	0	0
	HM[4](2_n3)	10.9	8.1
	HM[4](32_n)	16.1	15.1
	HM[4](32_r)	22.5	22.9

Graphics

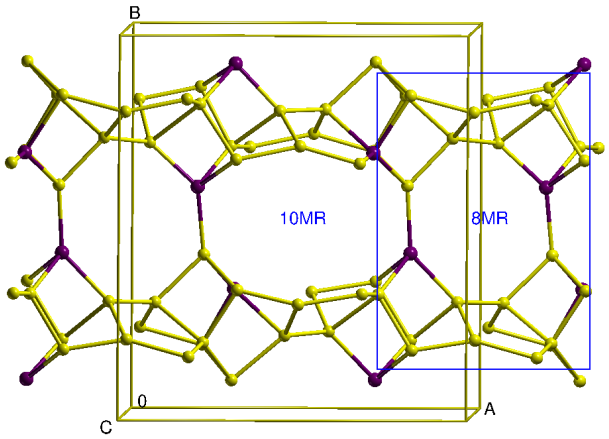

(a)

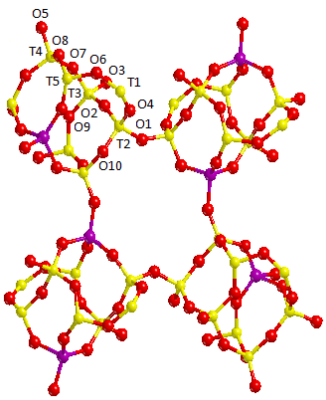

(b)

Figure 1: Acid Clinoptilolite. (a) Conventional cell; the primitive cell is shown within the blue rectangle. (b) Detailed representation of the unit cell without water molecules. Atoms belonging to the asymmetric unit are labelled according to the usual notation. The yellow, blue and red balls correspond to Si, Al and O atoms, respectively. Channels that run along the c axis, 8- and 10- MRs, respectively, are indicated. The water molecules and the acid site protons have been omitted.

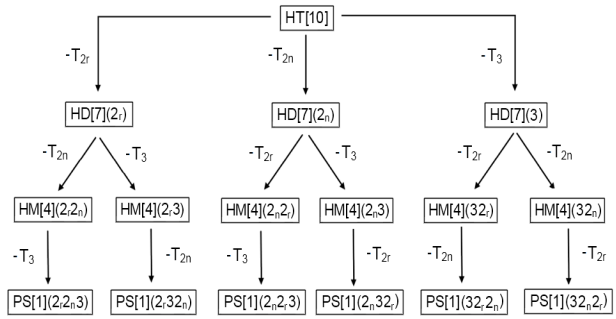

Figure 2: Scheme of the tree of reaction pathways involved in the dealumination process in decahydrated acid trialuminated HEU models. The starting H-CLI model and the intermediates involved in the dealumination reaction are indicated in the boxes. The arrows point toward the direction of the different processes considered. The T site from which the Al atom is abstracted in each event is represente on the arrows. Symbols are explained in the text.

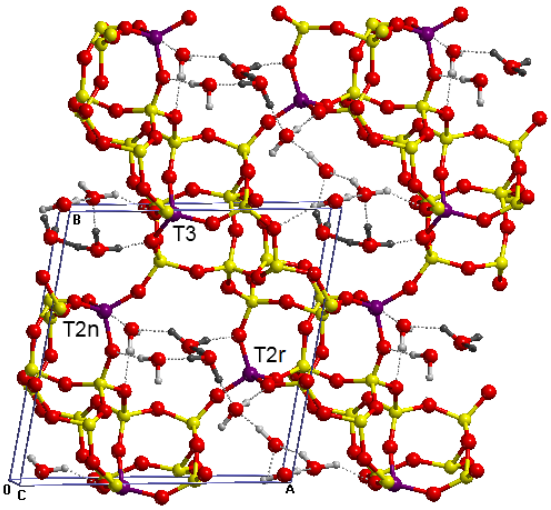

(a)

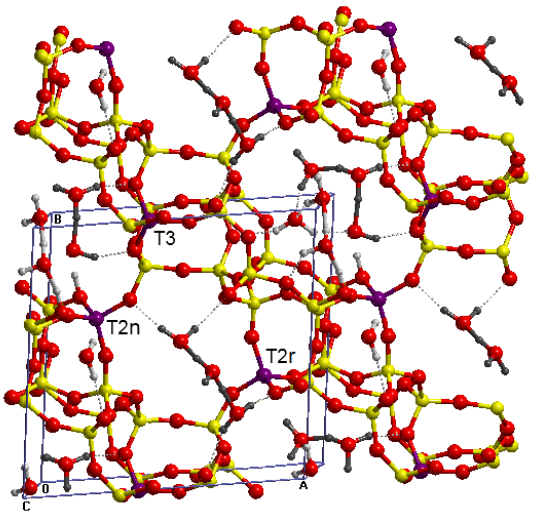

(b)

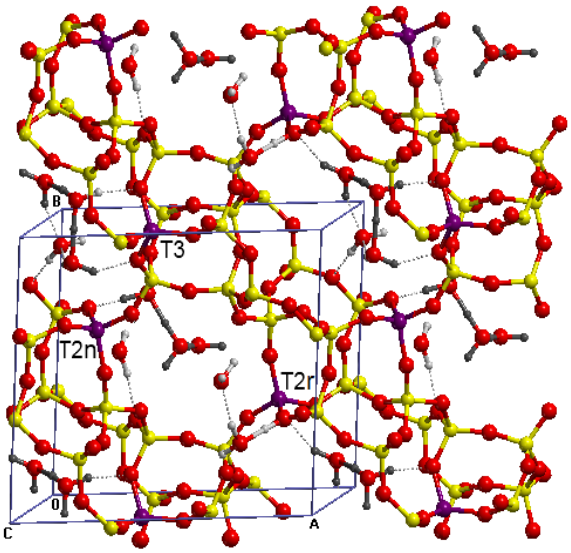

(c)

Figure 3: Decahydrated acid trialuminated HEU models. (a) HT[10]-1, (b) HT[10]-2 and (c) HT[10]-3. T-sites are indicated. The yellow, blue and red balls correspond to Si, Al and O atoms, respectively. The protons from the acid sites and the hydrogen atoms belonging to water molecules are in white and those corresponding to charged clusters are in dark gray.

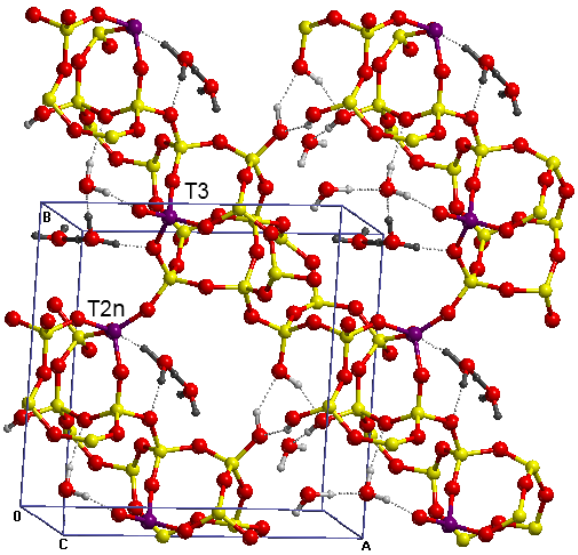

(a)

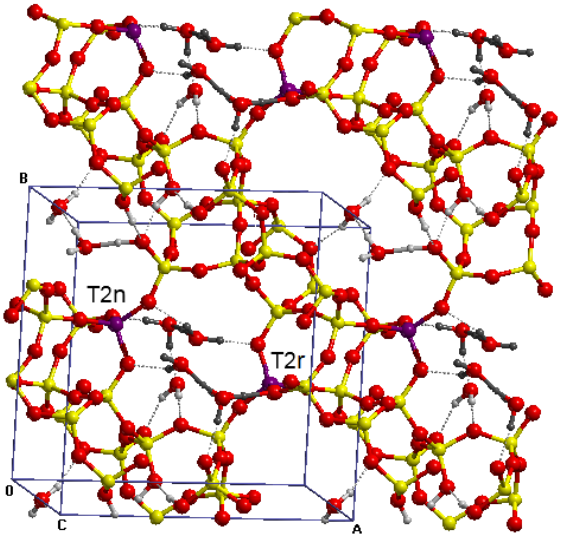

(c)

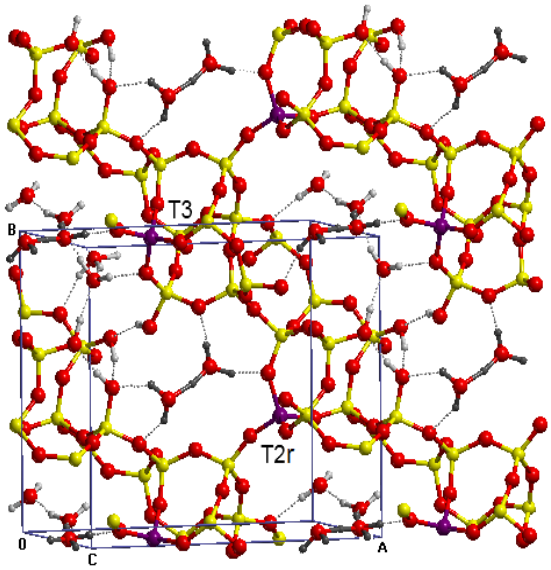

(b)

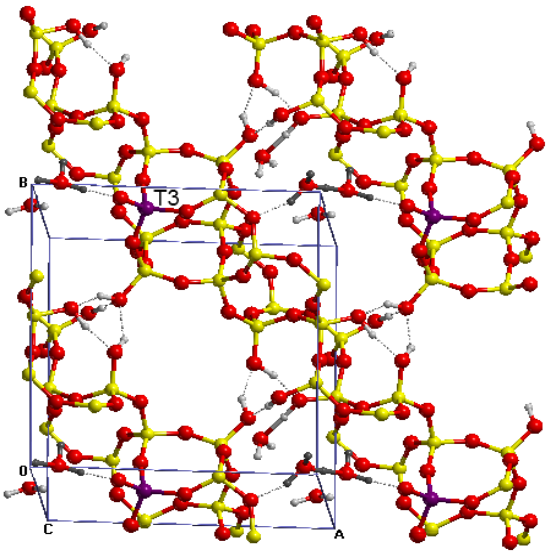

(d)

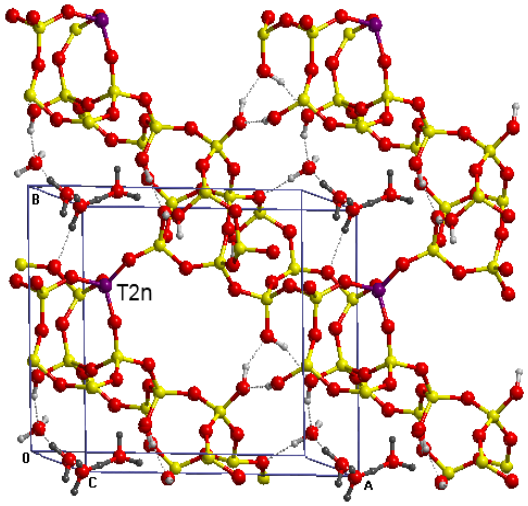

(e)

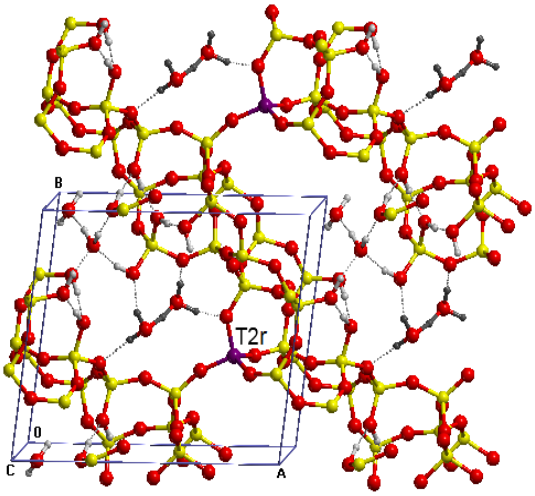

(g)

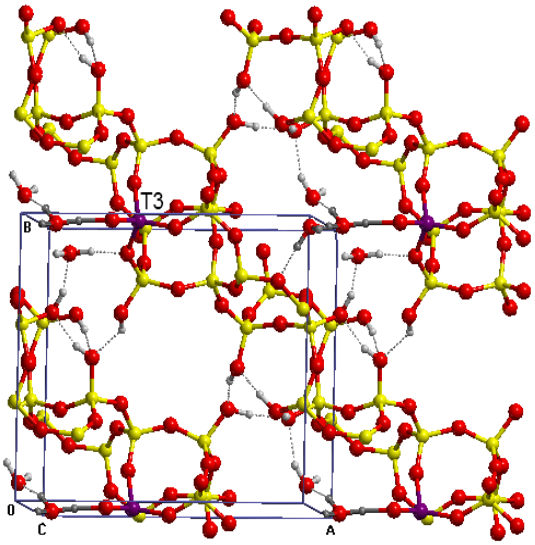

(f)

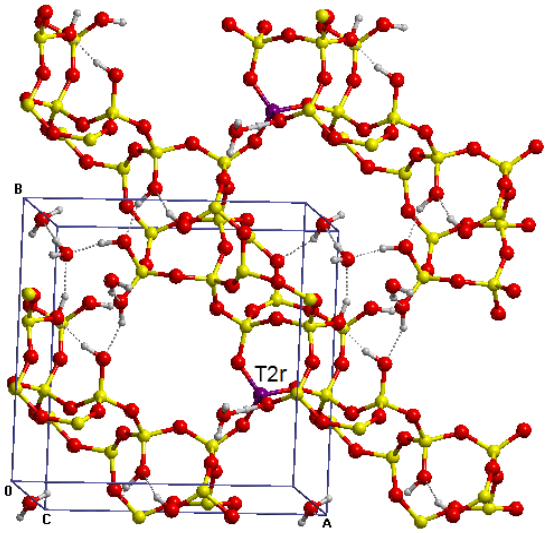

(h)

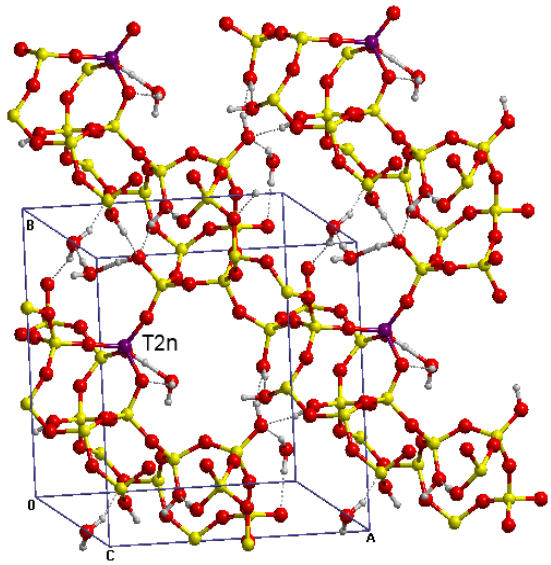

(i)

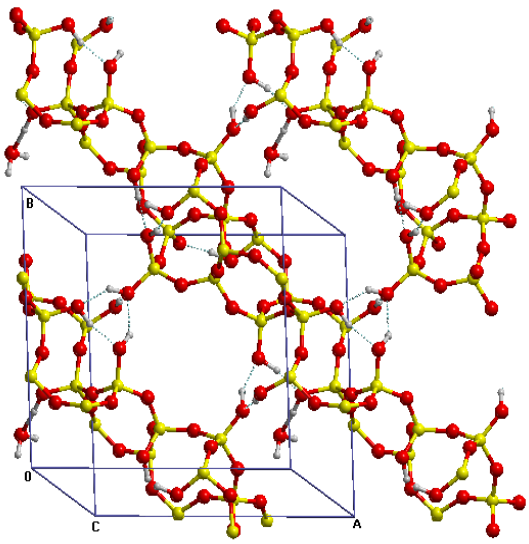

(j)

Figure 4: Models for the products of the dealumination of HT[10]-1. Step 1: (a) HD[7](2_t), (b) HD[7](2_n) and (c) HD[7](3). Step 2: (d) HM[4]($2,2_n$), (e) HM[4](2_t3), (f) HM[4](2_n2_t), (g) HM[4](2_n3), (h) HM[4](32_n) and (i) HM[4](32_t). Step 3: (j) PS[1] (2_t2_n3).

